J|A|C|S
ARTICLES
Published on Web 07/19/2002

Epitaxial Composite Layers of Electron Donors and Acceptors from Very Large Polycyclic Aromatic Hydrocarbons

Paolo Samorí,[†,§] Nikolai Severin,[†] Christopher D. Simpson,[‡] Klaus Müllen,*[,‡] and Jürgen P. Rabe*[,†]

Contribution from the Department of Physics, Humboldt University Berlin, Invalidenstrasse 110, 10115 Berlin, Germany, and Max-Planck-Institute for Polymer Research, Ackermannweg 10, 55128 Mainz, Germany

Received March 1, 2002

Abstract: Large polycyclic aromatic hydrocarbons (PAHs) can be considered as nanographenes, whose electron donating or accepting properties are controlled by their size and shape as well as functionalities in their periphery. Epitaxial thin films of them are targets for optoelectronic applications; however, large PAHs are increasingly difficult to process. Here we show that epitaxial layers of very large unsubstituted PAHs ($C_{42}H_{18}$ and $C_{132}H_{34}$), as well as a mixed layer of $C_{42}H_{18}$ with an electron acceptor, can be obtained by self-assembly from solution. The $C_{132}H_{34}$ is by far the largest nanographene that up to now has been processed into ordered thin films; due to its size it cannot be sublimed in a vacuum. Scanning tunneling microscopy (STM) studies reveal that the interaction with the substrate induces a strong perturbation of the electronic structure of the pure donor in the first epitaxial monolayer. In a second epitaxial layer with a donor acceptor stoichiometry of 2:1 the molecules are unperturbed.

Introduction

The fabrication of high-performance miniaturized molecular electronic devices based on conjugated (macro)molecules requires an accurate control both of the structural arrangement at the supramolecular level and of the electronic structure of the molecules composing the active organic matrix, ideally with a precision on the single molecule level.[1−8] Particularly mixed ordered layers of electron-rich and electron-poor conjugated molecules open new applications for molecular electronics.[9] Following the discovery of the high conductivity exhibited by iodine-doped polyacetylene,[10] a tremendous effort has been devoted to the processing of conjugated molecules in thin ordered films. One approach has been the sublimation in a vacuum,[11] which, although it allows to form crystalline organic layers, is severely limited by the size of the processable molecules. A second strategy that has been followed was processing from solutions. In this case, increasing the size of the rod- and disklike conjugated oligomers the intrinsic molecular conductivity increases with the number of unsaturated repeat units composing the molecule while, at the same time, the solubility decreases dramatically with the size of the molecule.[12] For solution processing the synthesis of conjugated (macro)-molecules with solubilizing side chains opened a pathway toward viable processability into thin films.[12,13] The side chains, however, lead to a dilution of the electronically active function of the molecule, and may also decrease the degree of conjugation due to a torsion of single bonds.[12]

Synthetic polycyclic aromatic hydrocarbons (PAHs), which can be regarded as two-dimensional subsections of graphite, constitute a class of π-conjugated compounds having various sizes and peripheral functionalities.[14−16] Unsubstituted PAHs have been processed only into ordered thin films by vacuum sublimation, with $C_{54}H_{22}$ being the largest reported case.[17] They

* Corresponding authors. Prof. Dr. K. Müllen: (e-mail) muellen@mpip-mainz.mpg.de. Prof. Dr. J. P. Rabe: (e-mail) rabe@physik.hu-berlin.de.
† Humboldt University Berlin.
§ Present address: Istituto per la Sintesi Organica e la Fotoreattività, C.N.R. Bologna, via Gobetti 101, 40129 Bologna, Italy.
‡ Max-Planck-Institute for Polymer Research.

(1) Bumm, L. A.; Arnold, J. J.; Cygan, M. T.; Dunbar, T. D.; Burgin, T. P.; Jones, L.; Allara, D. L.; Tour, J. M.; Weiss, P. S. *Science* **1996**, *271*, 1705−1707.
(2) Chen, J.; Reed, M. A.; Rawlett, A. M.; Tour, J. M. *Science* **1999**, *286*, 1550−1552.
(3) Langlais, V. J.; Schlittler, R. R.; Tang, H.; Gourdon, A.; Joachim, C.; Gimzewski, J. K. *Phys. Rev. Lett.* **1999**, *83*, 2809−2812.
(4) Friend, R. H.; Gymer, R. W.; Holmes, A. B.; Burroughes, J. H.; Marks, R. N.; Taliani, C.; Bradley, D. D. C.; Dos Santos, D. A.; Bredas, J. L.; Logdlund, M.; Salaneck, W. R. *Nature* **1999**, *397*, 121−128.
(5) Collier, C. P.; Mattersteig, G.; Wong, E. W.; Luo, Y.; Beverly, K.; Sampaio, J.; Raymo, F. M.; Stoddart, J. F.; Heath, J. R. *Science* **2000**, *289*, 1172−1175.
(6) Holmlin, R. E.; Ismagilov, R. F.; Haag, R.; Mujica, V.; Ratner, M. A.; Rampi, M. A.; Whitesides, G. M. *Angew. Chem., Int. Ed.* **2001**, *40*, 2316−2320.
(7) Schön, J. H.; Meng, H.; Bao, Z. *Nature* **2001**, *413*, 713−716.
(8) Cui, X. D.; Primak, A.; Zarate, X.; Tomfohr, J.; Sankey, O. F.; Moore, A. L.; Moore, T. A.; Gust, D.; Harris, G.; Lindsay, S. M. *Science* **2001**, *294*, 571−574.
(9) Schmidt-Mende, L.; Fechtenkotter, A.; Müllen, K.; Moons, E.; Friend, R. H.; MacKenzie, J. D. *Science* **2001**, *293*, 1119−1122.
(10) Chiang, C. K.; Fincher, C. R. J.; Park, Y. W.; Heeger, A. J.; Shirakawa, H.; Louis, E. J.; Gau, S. C.; MacDiarmid, A. G. *Phys. Rev. Lett.* **1977**, *39*, 1098−1101.
(11) Forrest, S. R. *Chem. Rev.* **1997**, *97*, 1793−1896.
(12) Müllen, K.; Wegner, G. *Electronic Materials: the Oligomeric Approach*; Wiley-VCH: Weinheim, Germany, 1998.
(13) Kraft, A.; Grimsdale, A. C.; Holmes, A. B. *Angew. Chem., Int. Ed.* **1998**, *37*, 402−428.
(14) Clar, E. *The Aromatic Sextet*; John Wiley: London, 1972.
(15) Watson, M. D.; Fechtenkotter, A.; Müllen, K. *Chem. Rev.* **2001**, *101*, 1267−1300.
(16) Samori, P.; Fechtenkotter, A.; Jackel, F.; Böhme, T.; Müllen, K.; Rabe, J. P. *J. Am. Chem. Soc.* **2001**, *123*, 11462−11467.

10.1021/ja020323q CCC: $22.00

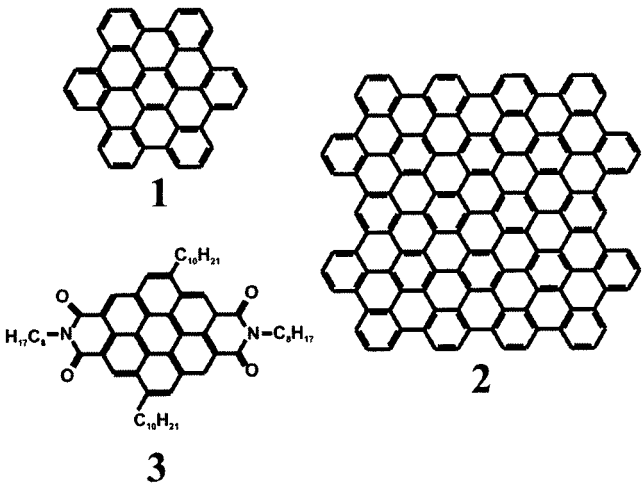

Figure 1. Chemical formulas of the PAHs: (**1**) hexa-*peri*-hexabenzocoronene ($C_{42}H_{18}$); (**2**) $C_{132}H_{34}$; and (**3**) alkylated coronenebis(dicarboximide) derivative.

are characterized by a high charge carrier mobility of the $\pi-\pi$ stacked supramolecular aggregates,[18] and when macroscopically processed in thin films in the presence of an acceptor, such as perylene dyes, they show high photovoltaic response with high external quantum efficiencies.[9]

Scanning Tunneling Microscopy makes it possible to probe the electronic states of the frontier orbitals of single molecules adsorbed on a flat conductive substrate providing a direct real-space imaging of the structures of organic monolayers with a submolecular resolution.[19,20]

Here we report the self-assembly of very large unsubstituted PAHs from solutions into epitaxial composites. STM is used at room temperature and ambient pressure to visualize these structures with submolecular resolution at the solution−graphite interface, as well as to investigate the electronic properties of the adsorbates on the single molecule scale.

Results and Discussion

The unsubstituted PAHs displayed in Figure 1, namely hexa-*peri*-hexabenzocoronene ($C_{42}H_{18}$, **1**) and $C_{132}H_{34}$ (**2**),[15] were dissolved in 1,2,4-trichlorobenzene (TCB) employing two different approaches: (i) solutions of neat **1** or **2** were kept at 100 °C for 12 h or (ii) an equimolar quantity of **1** or **2** and an alkylated coronenebis(dicarboximide)s derivative (**3**)[21] was solubilized. Saturated solutions of $C_{42}H_{18}$ with concentrations up to 10^{-4} M are obtained in this way (see Supporting Information), ready to be deposited on solid substrates. As currently used for conjugated polymers, the term solution is here employed in a broad sense with the meaning of dissolving single molecules or clusters thereof. The deposition on the substrate is characterized by a competition between adsorption and intermolecular clustering, being therefore a kinetically complicated process. While **1** and **2** are known to be strong electron donors, **3** exhibits the properties of a potent electron acceptor. In this case the strong homomolecular aggregation among **1** and **2** is likely to compete with the tendency to form acceptor−donor stacks, which might lead to an increased solubility of **1** and **2**.

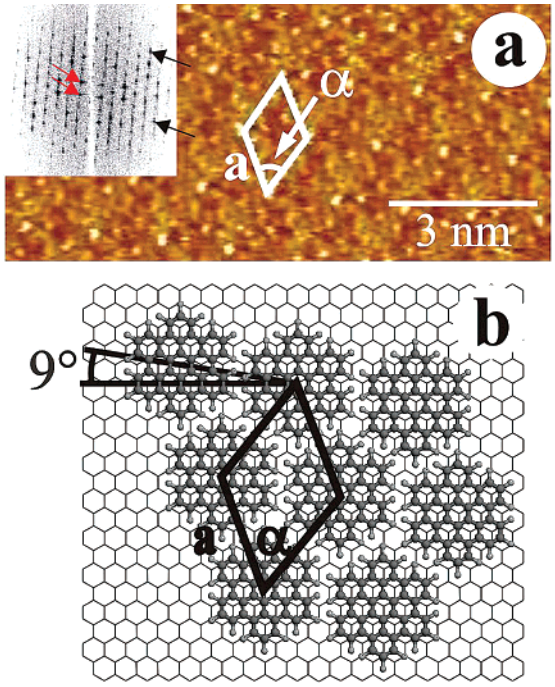

Figure 2. Hexagonally packed first layer of **1** adjacent to the substrate. (a) STM constant height images of **1** at the graphite−solution interface. The structure possesses a unit cell $a = (1.37 \pm 0.04)$ nm and $\alpha = (60 \pm 1)°$, leading to an area $A = (1.63 \pm 0.05)$ nm^2. The observed features do not reflect the frontier orbital of the neat $C_{42}H_{18}$. The measurements were performed on a sample of co-deposited **1** and **3** from solution. The 2D Fourier Transform in the inset provides evidence of the simultaneous visualization of the HOPG (black arrow) and adsorbate (red arrow) lattices. The packing model is displayed in part b. Tunneling condition of the STM image: (a) $U_t = 351$ mV, average $I_t = 436$ pA.

An STM image recorded at the interface between a solution and highly oriented pyrolitic graphite substrate (HOPG)[16] of a monolayer of **1** is shown in Figure 2a. The molecules pack in a crystalline structure with hexagonal symmetry (see model in Figure 2b), indistinguishable from the one detected for dry monolayers grown in ultrahigh vacuum.[22] The monolayer at the solid−liquid interface exhibits defect-free single crystals with areas larger than 10^4 nm^2, providing evidence for a strong adsorption on graphite. Moreover, due to the possibility of monitoring simultaneously the adsorbate and the substrate lattice, it is possible to achieve a spatial resolution of fractions of angstroms. This is evident in the 2D Fourier Transform in the inset of Figure 2a where the peaks of the HOPG lattice are indicated with the black arrows while those of the adlayer hexagonal arrangements are marked with red arrows.

Upon increasing the tunneling junction impedance, e.g. by changing the tunneling current in STM imaging, it is possible to lift the tip up from the substrate. This permits switching from the imaging of the first layer to the self-assembled structures of the second adsorbate layer, which are displayed in Figure 3a,c,e,f. For nondestructive measurements, these tunneling conditions can be used to estimate the average resistance of the complex molecule−solvent in the gap tip−substrate.[1] While for the first layer the tunneling impedance ranges from 2.7 ×

(17) Müller, M.; Peterson, J.; Strohmaier, R.; Gunther, C.; Karl, N.; Müllen, K.; *Angew. Chem., Int. Ed.* **1996**, *35*, 886−888.
(18) van de Craats, A. M.; Warman, J. M. *Adv. Mater.* **2001**, *13*, 130−133.
(19) Gimzewski, J. K.; Joachim, C. *Science* **1999**, *283*, 1683−1688.
(20) Yazdani, A.; Lieber, C. M. *Nature* **1999**, *401*, 227−230.
(21) Rohr, U.; Schlichting, P.; Bohm, A.; Gross, M.; Meerholz, K.; Brauchle, C.; Müllen, K. *Angew. Chem., Int. Ed. Engl.* **1998**, *37*, 1434−1437.
(22) Schmitz-Hübsch, T.; Sellam, F.; Staub, R.; Torker, M.; Fritz, T.; Kubel, C.; Müllen, K.; Leo, K. *Surf. Sci.* **2000**, *445*, 358−367.

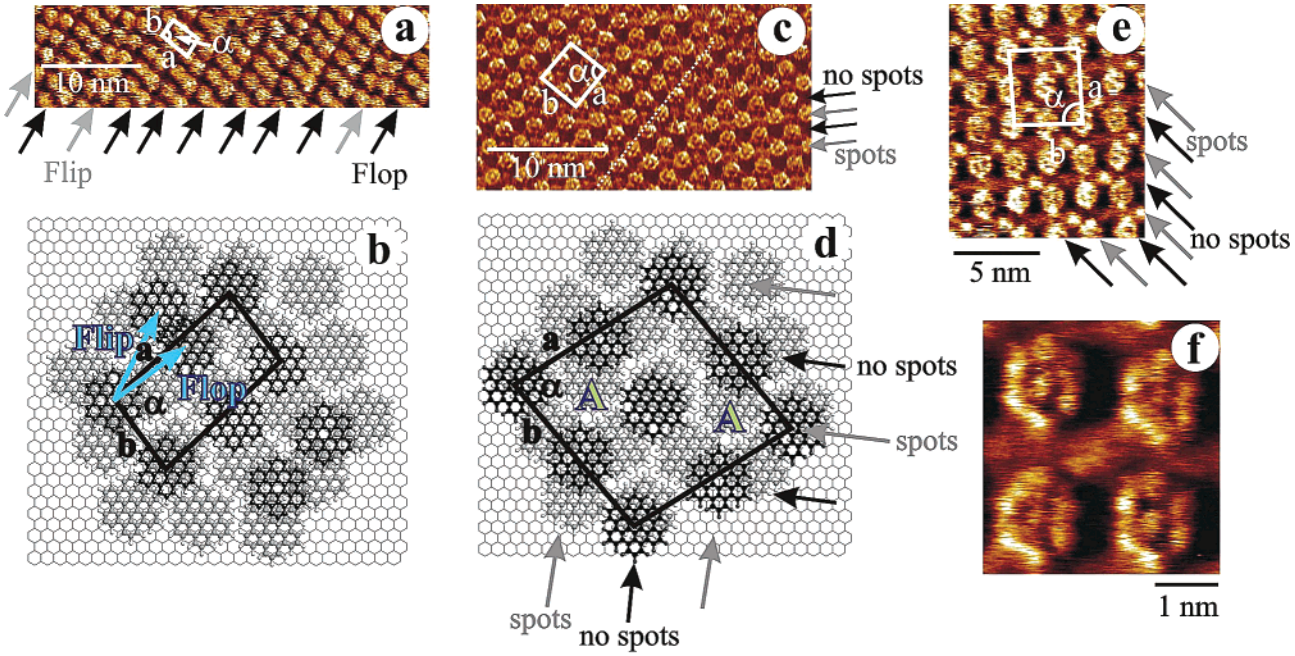

Figure 3. Self-assembled structures of the second layer of **1**. (a, c, e, f) STM constant height images at the graphite−solution interface. (a) Dimer structure resolved on a film prepared by depositing a pure solution of **1**. The unit cell dimensions are $a = (3.3 \pm 0.2)$ nm, $b = (1.82 \pm 0.15)$ nm, $\alpha = (86 \pm 5)°$, and $A = (6.0 \pm 0.5)$ nm^2. A "flip-flop" arrangement of the dimer structure exists, denoting an energetic similarity. (c, e, f) display the oblique arrangement of a film prepared by co-deposition of **1** and **3**. The unit cell dimensions are $a = (3.7 \pm 0.3)$ nm, $b = (3.6 \pm 0.3)$ nm, $\alpha = (86 \pm 5)°$, and $A = (3.3 \pm 0.3)$ nm^2. In part c alternate rows bearing coadsorbed **3** (depicted with a white spot among two $C_{42}H_{18}$ molecules) are indicated by gray arrows. Albeit the vacancies between the $C_{42}H_{18}$ molecules in the diagonals of the oblique structure have the same size, **3** packs only every second row probably because of its preferential adsorption on the electron donor disk of **1**, which is exposed in the underlying first $C_{42}H_{18}$ layer. In the images in parts c and e, the contrasts reflect accurately the nodal planes of the frontier orbitals of the neat $C_{42}H_{18}$, as evident in part f. The models of the dimer and oblique packing are displayed in parts b and d, respectively. The immobilization of the molecules at surfaces was smaller for the second than for the first layer (Figure 2), leading to larger error bars in the determined unit cell and to a less accurate precision in the modeling. Tunneling condition of the STM images: (a) $U_t = 1020$ mV, average $I_t = 122$ pA. (c) $U_t = 279$ mV, average $I_t = 155$ pA. (e, f) $U_t = 1250$ mV, average $I_t = 125$ pA.

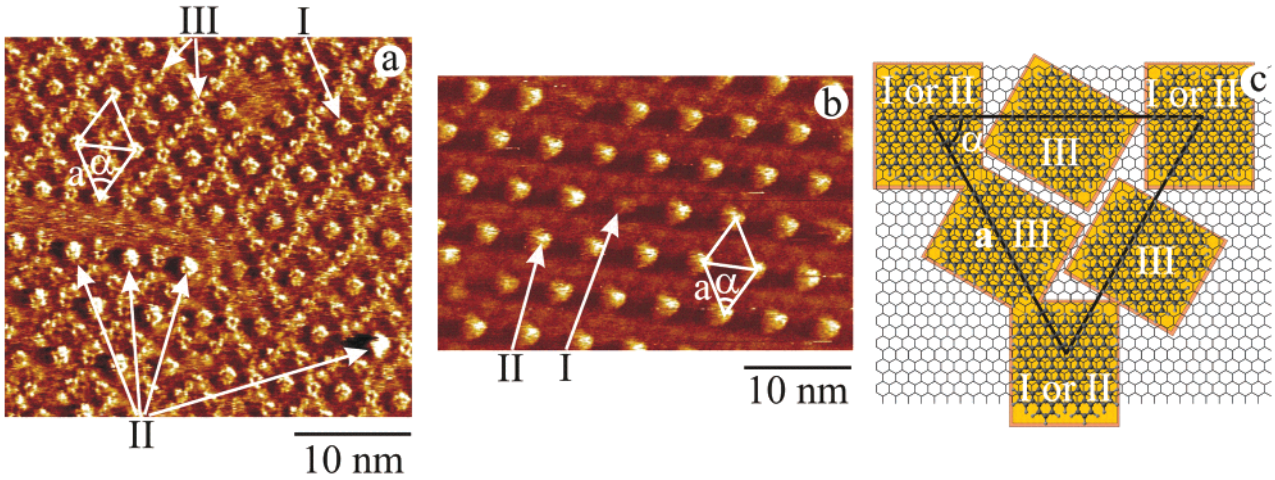

Figure 4. Hexagonal architecture of **3**. (a, b) STM constant height images of a film of **3** at the graphite−solution interface from a neat solution of **3**. Three different types of contrast representing the disks can be observed (I−III). The unit cell is given by $a = (5.2 \pm 0.3)$ nm, $\alpha = (60 \pm 3)°$, and $A = (23 \pm 4)$ nm^2. The absence of side chains which could induce the molecule to lose a geometrical planarity suggests that, differently from ref 16, the molecules are allowed to acquire the same position along the *Z*-axis in the gap tip−substrate. Since the molecules of types I and II appear to be packed in the same location in the plane relative to the graphite, the different contrasts I and II are probably due to a different number of stacked $C_{42}H_{18}$ molecules in the gap tip−substrate. The packing model, with the error bar painted a different color, is shown in part c. (a) $U_t = 1000$ mV, average $I_t = 94$ pA. (b) $U_t = 1500$ mV, average $I_t = 60$ pA.

10^7 to 1.7×10^9 Ω, for the second layer, since the electrons need to tunnel through a bilayer, it extends from 1.1×10^9 to 8.4×10^9 Ω. In the second layer, the samples prepared from neat **1** (procedure i) exhibit a dimer structure (Figure 3a,b) consisting of tightly packed $C_{42}H_{18}$ disks, while the films prepared by co-deposition of **1** and **3** (procedure ii) exhibit an oblique arrangement (Figure 3c−f). This latter structure is a complex architecture: within the same layer between two physisorbed $C_{42}H_{18}$ disks, along the gray arrows in Figure 3c−e a white spot can be recognized and ascribed to a coadsorbed molecule **3**. Notably, in both the oblique and dimer structures the high-resolution images allow the recognition of an intramolecular contrast that seems to reflect the symmetry of the nodal plane of the frontier π-orbitals of the $C_{42}H_{18}$ molecule, namely

one central bright spot surrounded by 6 other equidistant spots located at the edges of a hexagon, as evidenced in Figure 3f.

The different contrasts of the $C_{42}H_{18}$ molecules visualized by STM in the first and in the second layer (Figures 2a and 3a,c,e,f, respectively) unambiguously manifest a different electronic structure of the molecule in the two configurations. In the first case, to maximize the gain in enthalpy acquired with the adsorption at the surface,[23] the $C_{42}H_{18}$ molecules arrange into an extremely tightly packed structure. Molecular Mechanics calculations computed in a vacuum environment with use of a pcff force field[24] reveal that the first external rim of carbon atoms in the $C_{42}H_{18}$ molecules in the hexagonal arrangement is bent away from the surface. This effect, possibly together with the strong interaction between the $C_{42}H_{18}$ and the HOPG surface, leads to a significant perturbation of the electronic states of the $C_{42}H_{18}$. In the latter case, characterized by a larger distance between the visualized molecule and the substrate, the observed contrast provides a genuine image of the local densities of states of the frontier orbitals of the neat $C_{42}H_{18}$ (Figure 3f). The decoupling of the electronic states of the molecule from those of the substrate is likely to be further enhanced by the variation of the packing symmetry from the hexagonal arrangement.

The deposition of **1** by drop casting diluted solutions (ca. 10^{-6} M) in hot TCB makes it possible also to produce *dry* monolayers of the hexagonally packed $C_{42}H_{18}$ arrangement. These monolayers exhibit a striking stability in an air environment and could be visualized with STM. Notably, this stable electron-donor monolayer can be used as a template for subsequent surface functionalizations.

Comparing the two procedures i and ii exploited successfully for the solubilization of the $C_{42}H_{18}$, procedure ii allows to self-assembly of the stable double layers, while with strategy i a second $C_{42}H_{18}$ layer exhibits a high molecular diffusion on the time scale of the STM measurements since it cannot be imaged. This indicates that the acceptor, which co-crystallizes with the $C_{42}H_{18}$ in the oblique arrangement, stabilizes the overall structure of the second layer. Note also the better resolved intramolecular patterns in the oblique arrangement of Figure 3e as compared to the dimers of Figure 3a.

The solubilization in hot TCB (procedure i) is successful also for the giant PAH consisting of 132 aromatic carbons (**2**). This compound is processed into crystalline monolayers which are visualized by STM (Figure 4a,b). The adsorbate is characterized by a hexagonal arrangement with a lattice vector of $a = (5.2 \pm 0.3)$ nm. The 2D unit cell comprises 4 molecules per unit cell: one of them (indicated by I and II in Figure 4a,b) at the corner of the unit cell and on the sides (marked III in Figure 4a), leading to two different types of complexes of molecule−HOPG with different electronic properties. This interpretation is confirmed by the different change of contrast of I, II, and III upon variation of the tunneling parameters from Figure 4a to Figure 4b. It is likely that I and II differ from the number of disks which are stacked in the gap tip−substrate. While the arrangement shown in the model in Figure 4c appears to be loosely packed, it is consistent with the STM measurements. It probably implies the coadsorption of solvent molecules which could not be detected because of their conformational mobilities that are faster than the STM scanning rate. Molecule **2**, which due to the extended π-electron delocalization in 2D has electronic properties approaching those of graphite, represents the so far largest unsubstituted conjugated molecule that was not only solubilized, but also processed on a surface into highly ordered structures, if we exclude carbon nanotubes [25,26] which do not suffer from strong $\pi-\pi$ intermolecular interactions inducing aggregations. The very large size of this molecule, which is the largest nanographene that was ever processed into ordered thin films, does not permit sublimation in a vacuum.

Conclusions and Outlooks

The solubilization of the nanographenes is of more general importance, e.g. for their purification as well as their characterization with wet analytical techniques. Moreover the epitaxial thin films are attractive for many technological applications. An epitaxial thin film of very large fully conjugated unsubstituted molecular systems, because of the absence of the side chains, represents a good candidate for the fabrication of high-performance electronic devices. Furthermore, structures of mixed epitaxial layers of electron acceptors (A) and donors (D) provide access to the STM exploration of the electron transfer in noncovalently linked individual A−D pairs as an alternative to the covalently bonded ones.[27] Finally, the processing described here may be applied to other molecules with sizes which do not allow high-vacuum-sublimation processing, also including polymers.

Acknowledgment. We are grateful to Xiaomin Yin for the UV−vis spectroscopy measurements and Thilo Böhme for the Molecular Mechanics calculations. This work was supported by EU-TMR project SISITOMAS, the Volkswagen-Stiftung (Elektronentransport durch konjugierte molekulare Scheiben und Ketten), the European Science Foundation through SMARTON, and the German "Bundesministerium fuer Forschung und Technologie" as part of the program "Zentrum fuer multifunktionelle Werkstoffe und miniaturisierte Funktionseinheiten".

Supporting Information Available: UV−vis absorption spectrum of $C_{42}H_{18}$ in 1,2,4-trichlorobenzene (PDF). This material is available free of charge via the Internet at http://pubs.acs.org.

JA020323Q

(23) Samori, P.; Severin, N.; Müllen, K.; Rabe, J. P. *Adv. Mater.* **2000**, *12*, 579−582.
(24) Molecular modelling package Discover, Version 4.0.0; Biosym. Technologies Inc.: San Diego, CA.
(25) Dekker: C. *Phys. Today* **1999**, *52*, 22−28.
(26) Ebbesen, T. W. *Phys. Today* **1996**, *49*, 26−32.
(27) Davis, W. B.; Svec, W. A.; Ratner, M. A.; Wasielewski, M. R. *Nature* **1998**, *396*, 60−63.